Journal of Power Sources 195 (2010) 3579–3589

Contents lists available at ScienceDirect

Journal of Power Sources

journal homepage: www.elsevier.com/locate/jpowsour

Heat-up and start-up modeling of direct internal reforming solid oxide fuel cells

C. Ozgur Colpan[a,*], Feridun Hamdullahpur[b], Ibrahim Dincer[c]

[a] Mechanical and Aerospace Engineering Department, Carleton University, 1125 Colonel by Drive, Ottawa, Ontario, Canada K1S 5B6
[b] Mechanical and Mechatronics Engineering Department, University of Waterloo, 200 University Avenue West, Waterloo, Ontario, Canada N2L 3G1
[c] Faculty of Engineering and Applied Science, University of Ontario Institute of Technology, 2000 Simcoe Street North, Oshawa, Ontario, Canada L1H 7L7

ARTICLE INFO

Article history:
Received 13 November 2009
Accepted 6 December 2009
Available online 21 December 2009

Keywords:
Solid oxide fuel cell
Internal reforming
Transient
Start-up
Thermomechanical
Failure

ABSTRACT

In this paper, a transient heat transfer model to simulate the heat-up and start-up periods of co- and counter-flow direct internal reforming solid oxide fuel cells is developed and presented. In this comprehensive model, all the heat transfer mechanisms, i.e. conduction, convection, and radiation, and all the polarization nodes, i.e. ohmic, activation, and concentration, are considered. The heat transfer model is validated using the results of a benchmark test and two numerical studies obtained from the literature. After validating the model, the heat-up, start-up, and steady-state behaviors of the cell are investigated. In addition, the first principal thermal stresses are calculated to find the probability of failure of the cell during its operation. The results of the present model are in good agreement with the literature data. It is also shown for the given input data that counter-flow case yields a higher average current density and power density, but a lower electrical efficiency of the cell. For the temperature controlled heat-up and start-up strategy, the maximum probability of failure during the operation of the cell is found to be 0.068% and 0.078% for co- and counter-flow configurations, respectively.

1. Introduction

Solid oxide fuel cell (SOFC) is an electrochemical conversion device that can be designed to operate in temperatures ranging from 500 °C to 1000 °C. The main application area of SOFC is stationary power and heat generation. However, it can be used in some portable applications, e.g. power generator for camping, and transportation applications, e.g. auxiliary power unit for automobiles. It has several advantages compared to low temperature fuel cells, e.g. proton exchange membrane fuel cell (PEMFC) and direct methanol fuel cell (DMFC). These advantages can be listed as simplicity in design concept since only gas and solid phases exist, fuel flexibility, internal reforming of the fuel, and integration with other systems, e.g. gas turbine and gasification system. However, there are challenges with construction and durability due to its high temperature; and carbon deposition can be a problem if the fuel cell system is not properly designed. For preventing the carbon deposition, solutions such as adjusting the steam to carbon ratio at the fuel channel inlet and selecting appropriate materials for electrodes can be considered.

The heat-up and start-up periods of a SOFC should be considered as one of the most crucial parts of the operation of the fuel cell, especially for portable and transportation applications, mainly because of the considerable amount of time passed in these periods. Different operating strategies can be followed in these periods. For example, for the heat-up period, the air channel can be fed by hot air, e.g. Ref. [1] or exhaust gases from a burner, e.g. Ref. [2]. For the start-up period, the inlet temperature of the gas channels can be fixed or controlled, e.g. Ref. [1], or a stepwise increment of current density can be applied, e.g. Ref. [3]. In this paper, one of the most common operating strategies for the heat-up and start-up periods is used, which is explained as follows. In the heat-up period, the temperature of the cell is increased up to a point that is high enough to produce a meaningful amount of power. In this period, only air is sent through the air channel with a stepwise increase in temperature. This increase should be done taking into account thermomechanical considerations not to cause excessive internal stresses. As the heat-up period ends, start-up period, in which air and fuel are both continuously fed to the cell at a fixed temperature, begins. This period continues until the cell reaches the steady-state condition. The minimization of the duration of the time passed in these periods is an important design consideration. The first step in this consideration is the prediction of the performance of the fuel cell in these periods, which can be done through numerical modeling.

There are different SOFC models in cell, stack and system levels in the literature. Different considerations can be taken into account in these models depending on the purpose of the modeling. According to the choice of the spatial domain, 0D, 1D, 2D, and 3D models can be developed. For example, in the paper by

* Corresponding author. Tel.: +1 613 5202600x8257; fax: +1 613 520 5715.
E-mail address: cocolpan@connect.carleton.ca (C.O. Colpan).

0378-7753/$ – see front matter © 2009 Elsevier B.V. All rights reserved.
doi:10.1016/j.jpowsour.2009.12.021

Nomenclature

A	cross-sectional area, cm^2
c_p	specific heat at constant pressure, $J\,g^{-1}\,K^{-1}$
D	diffusivity, $cm^2\,s^{-1}$
F	Faraday constant, C
$\bar{g}$	specific molar Gibbs free energy, $J\,mole^{-1}$
h	heat transfer coefficient, $W\,cm^{-2}\,K^{-1}$
$\bar{h}$	specific molar enthalpy, $J\,mole^{-1}$
$\dot{H}$	enthalpy flow rate, W
i	current density, $A\,cm^{-2}$
i_o	exchange current density, $A\,cm^{-2}$
k	thermal conductivity, $W\,cm^{-1}\,K^{-1}$
L	length of the cell, cm
LHV	lower heating value, $J\,mole^{-1}$
M	molecular weight, $g\,mole^{-1}$
$\dot{n}$	molar flow rate, $mole\,s^{-1}$
P	pressure, bar
P_f	failure probability
$\dot{q}$	heat transfer rate, W
$\dot{r}$	conversion rate, $mole\,s^{-1}$
R	universal gas constant, $J\,mole^{-1}\,K^{-1}$
Re_{D_h}	Reynolds number in an internal flow
t	time, s; thickness, cm
T	temperature, K
U_F	fuel utilization ratio
V	voltage, V; volume, cm^3
V_o	reference volume, cm^3
V_v	porosity
w	width, cm
$\dot{W}$	power output, W
x	molar concentration

Greek letters

ρ	electrical resistivity of cell components, Ω cm; mass density, $g\,cm^{-3}$
η_{el}	electrical efficiency
λ_{air}	excess air coefficient
τ	tortuosity
μ	viscosity, $g\,s^{-1}\,cm^{-1}$
α	thermal diffusivity, $cm^2\,s^{-1}$
σ	first principal thermal stress, MPa
σ_o	characteristic strength, MPa

Subscripts

a	anode; air
ac	air channel
act	activation
ai	anode interconnect
ave	average
c	cathode; convection
ci	cathode interconnect
conc	concentration
e	electrolyte
el	electrochemical; electrical
fc	fuel channel
fi	fuel channel inlet
ohm	ohmic
mix	mixture
N	Nernst
o	standard
PEN	positive/electrolyte/negative
prod	product
r	reaction; radiation
react	reactant
s	solid structure
str	steam reforming reaction for methane
w	wall
wgs	water gas shift reaction

Superscripts

b	bulk
o	standard state

Colpan et al. [4], the development of a 0D model of a direct internal reforming SOFC (DIR-SOFC) was presented; and the effect of recirculation ratio and fuel utilization ratio on the air utilization ratio, cell voltage, power output, and electrical efficiency of the cell was discussed. According to the choice of the temporal domain, steady-state and transient models can be developed. Transient modeling should be conducted if any of the following or combination of them is simulated: heat-up, start-up, shut-down and load change. For example, in the paper by Li et al. [5], the effect of step changes in fuel flow rate, air flow rate, and stack voltage on the performance of a cross-flow DIR-SOFC was discussed. Thermomechanical modeling is used to calculate the stresses formed inside the fuel cell. For example, in the study by Yakabe et al. [6], the internal stresses in a cell were estimated as a function of the cell size, the operating voltage, and the thermal conductivity of the cell components. Carbon deposition models are used to prevent the carbon deposition at the anode catalyst. For example, Farhad and Hamdullahpur [7] formed carbon deposition boundary curves based on thermodynamic equilibrium as a preliminary step to develop fuel maps. In system level modeling, integration of SOFC with other systems are studied using thermodynamic and economic tools such as energy, exergy, and thermoeconomic analyses. For example, Colpan et al. [8] investigated the integration of a SOFC with a charcoal fueled updraft gasifier. In another follow-up paper [9], they studied the effect of gasification agent on the performance on an integrated SOFC and biomass gasification system. More information on the different types of SOFC models can be found in a review paper by Colpan et al. [10].

In the literature, few studies on the modeling of heat-up and start-up periods are available. However, heat transfer mechanisms and/or polarizations were not fully covered in these models. For example, Selimovic et al. [1] studied the transient, e.g. heat-up, start-up, and shut-down, and steady state operations of SOFC through numerical modeling to determine the stresses caused by the difference in thermal expansion coefficients. In their model, they assumed the solid temperature as homogeneous in each volume element; and they used a simple assumption for the polarizations. They assumed that the sum of activation and concentration polarizations at each of the electrode is equal to the ohmic loss in the electrolyte. Petruzzi et al. [2] developed a model to simulate the heat-up and start-periods of a SOFC to be used as an auxiliary power unit for automobiles. They produced time-dependent profiles of temperature, current, power density, and gas concentrations. Their model was limited to cross-flow configuration and they neglected concentration polarization. Damm and Fedorov [11] developed 1D SOFC models to generate time-dependent temperature profiles during heat-up and start-up periods. They neglected radiation heat transfer and used a simple relation for polarization, which is mainly a function of porosity, in their model.

The thermal stresses formed during the heat-up and start-up periods of a cell are of great practical importance since these stresses could cause a failure in the operation of the cell and/or

affect the performance drastically. Due to this fact, the design of a SOFC and the determination of the right strategy for its transient operation should be done by taking into account the thermomechanical considerations. In the literature, these considerations are generally included in the modeling in three ways: checking the maximum temperature gradient, e.g. Ref. [12], checking the maximum principal stresses, e.g. Ref. [1], or calculating the failure probability, e.g. Refs. [13–16]. Among them, the last one, which is based on a statistical approach, gives a better estimation for the effect of thermal stresses on the operation of a SOFC.

The objective of this study is to develop a comprehensive model to study the heat-up and start-up periods of co- and counter-flow DIR-SOFCs. For this purpose, a quasi 2D and transient heat transfer model of planar DIR-SOFCs is developed. This model includes all the heat transfer mechanisms, i.e. conduction, convection, and radiation, and all the polarization nodes, i.e. ohmic, activation, and concentration. In the first part of this study, the model is validated with the results of a benchmark test and two models found in the literature; and the transient behavior of the cell is studied for the co- and counter-flow configurations to understand the phenomena better. In the second part of this study, the first principal thermal stresses formed during the operation of the cell are calculated; and then these stresses are used to calculate the probability of failure of the cell during its operation.

2. Modeling

In this study, a quasi 2D transient heat transfer model is developed to study the heat-up and start-up periods of co- and counter-flow DIR-SOFCs. In modeling the heat-up period, only the heat transfer equations are solved since there is no flow in the fuel channel. As followed in the study by Selimovic et al. [1], the air channel inlet temperature is increased by 100 °C more than the minimum solid temperature throughout this period not to generate large stresses. In modeling the start-up period, continuity equations are first solved for the air and fuel channels. The source terms in these equations are found solving the relation between the cell voltage and the polarizations, chemical equilibrium relation for water–gas shift reaction, and chemical kinetics of steam reforming reaction. Solving the continuity equations, the obtained are the molar flow rate and composition of the gas species, and the current density distribution. These data and the temperature distribution known from the previous time step are used in the heat transfer equations to calculate the temperature distribution in the next time step. Iterations continue until the system reaches the steady-state condition. This condition is satisfied when absolute temperature difference between the two consecutive time steps for each node becomes less than a threshold value, which is chosen as 10^{-4} in this study. The main features and assumptions of this model are listed below:

- The input parameters of the model are cell voltage, Reynolds number at the fuel channel inlet, excess air coefficient, cell geometry, properties of materials, ambient temperature, molar composition at the fuel and air channel inlets, mass flow rate of air for the heat-up period, and cell pressure.
- The output parameters of the model are heat-up and start-up time, distributions of current density, temperature and molar gas composition, fuel utilization, power output and electrical efficiency of the cell.
- A control volume around the repeat element found in the middle of a planar SOFC stack, as shown in Fig. 1, is taken; and it is assumed that the solid structure has adiabatic boundary conditions due to the symmetry.

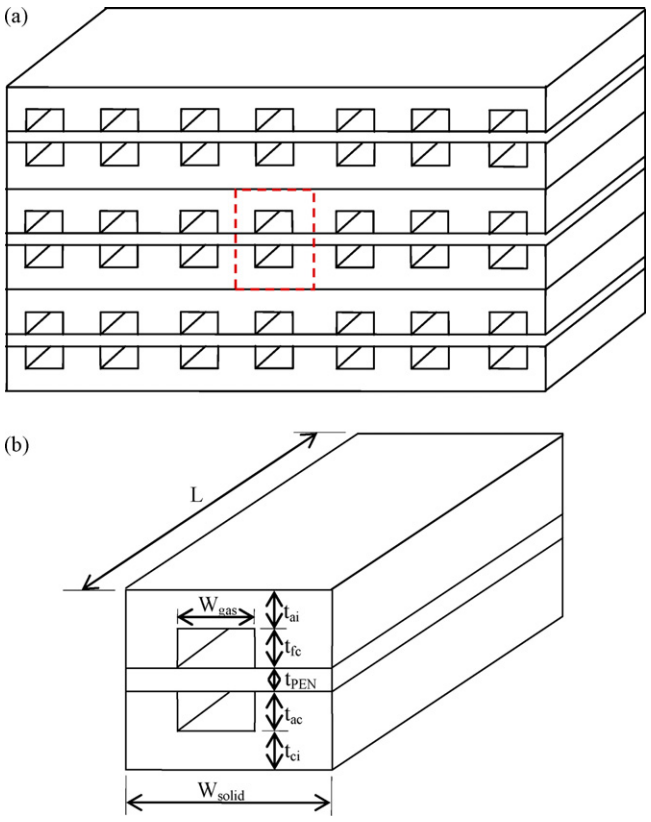

Fig. 1. Schematic of (a) the planar SOFC stack and (b) the repeat element found in the middle of the stack.

- Solid structure is modeled in 2D; whereas gas channels are modeled in 1D.
- Six gas species, namely CH_4, H_2, CO, CO_2, H_2O and N_2, are considered at the fuel channel inlet; and two gas species, namely O_2 and N_2, are considered at the air channel inlet.
- Fully developed laminar flow conditions are assumed in the gas channels.
- Natural convection at the heat-up period, forced convection at the start-up period, surface-to-surface radiation effects, conduction heat transfer within the solid structure including the section where the interconnects are in contact with positive/electrolyte/negative (PEN) structure are taken into account in the modeling.
- All polarizations, i.e. ohmic, activation and concentration, are considered.
- A finite difference method is used for numerical calculations.
- A computer code using Matlab is developed for the solution of the modeling equations.

In a DIR-SOFC, steam reforming reaction, water–gas shift reaction, and electrochemical oxidation of hydrogen as given in Eqs. (1)–(3), respectively, occur. Note that the direct oxidation of carbon monoxide is not included in the modeling; but it is assumed that this gas first converts into hydrogen via Eq. (2) and then it is oxidized:

$$CH_4 + H_2O \leftrightarrow CO + 3H_2 \quad (1)$$

$$CO + H_2O \leftrightarrow H_2 + CO_2 \quad (2)$$

$$H_2 + (1/2)O_2 \rightarrow H_2O \quad (3)$$

Based on the reactions shown above, the continuity equations at the fuel and air channels are shown in Table 1. Heat transfer equations are written for each control volume enclosing the compo-

Table 1
Continuity equations.

Control volume	Continuity equations
Fuel channel	$\frac{d\dot{n}''_{CH_4}}{dx} = \frac{-\dot{r}''_{str}}{t_{fc}}$
	$\frac{d\dot{n}''_{H_2}}{dx} = \frac{3\dot{r}''_{str}}{t_{fc}} + \Delta\dot{n}'''_{wgs} - \frac{\dot{r}''_{el}}{t_{fc}}$
	$\frac{d\dot{n}''_{CO}}{dx} = \frac{\dot{r}''_{str}}{t_{fc}} - \Delta\dot{n}'''_{wgs}$
	$\frac{d\dot{n}''_{CO_2}}{dx} = \Delta\dot{n}'''_{wgs}$
	$\frac{d\dot{n}''_{H_2O}}{dx} = \frac{-\dot{r}''_{str}}{t_{fc}} - \Delta\dot{n}'''_{wgs} + \frac{\dot{r}''_{el}}{t_{fc}}$
	$\frac{d\dot{n}''_{N_2}}{dx} = 0$
Air channel	$\frac{d\dot{n}''_{O_2}}{dx} = \frac{-\dot{r}''_{el}/2}{t_{ac}}$
	$\frac{d\dot{n}''_{N_2}}{dx} = 0$

nents of the cell, as shown in Table 2. These components are anode interconnect, fuel channel, PEN, air channel and cathode interconnect. The auxiliary relations used in the continuity and heat transfer equations are given in Table 3.

3. Probability analysis of failure

One of the main failure modes for a SOFC is the fracture of PEN because of the thermal stresses formed during its operation. The main reason of the formation of these stresses is the mismatch between the thermal expansion coefficients of the components of the PEN, i.e. anode, electrolyte, and cathode. These components are also brittle because of their ceramic nature.

In modeling, the first principal thermal stress distributions in the components of the PEN are first found. For this purpose, a commercial software package (so-called: Comsol Multiphysics) is used for calculating these stresses formed in the components of the PEN. The temperature distribution found using the transient heat transfer model is defined as a function in this software. It is assumed that the materials are isotropic and the components could deform freely; i.e. free constraint condition. After finding the thermal stress distributions, the Weibull approach [21] is used to calculate the failure probability of the components as given in Eq. (4):

$$P_f^k = 1 - \exp\left(-\int_{V_k}\left(\frac{\sigma_k}{\sigma_{k,o}}\right)^m \cdot \frac{dV_k}{V_{k,o}}\right) \quad (4)$$

where k denotes anode, electrolyte or cathode.

This equation can be written for the 2D modeling technique as used in this paper, and constant values of characteristic strength, σ_o, and reference volume, V_o, as shown in Eq. (5):

$$P_f^k = 1 - \exp\left(-\frac{W_{solid}}{\sigma_{k,o}^m \cdot V_{k,o}} \cdot \int_{A_k}\sigma_k^m \cdot dA_k\right) \quad (5)$$

Material properties of the components of the PEN are shown in Table 4. It should be noted that these properties are assumed to be constant during the heat-up and start-up periods of the cell.

4. Results and discussion

In this section, a validation of the heat transfer model using the results of the benchmark test [22] and two models [1,23] found in the literature is first presented. Then, the transient and steady-state behaviors of the cell are discussed through the results. Finally, the first principal thermal stress distributions and the failure probability for the co- and counter-flow DIR-SOFCs are shown and discussed.

4.1. Validation

The validation of the model is done using the results of the benchmark test, which was conducted in a workshop organized

Table 2
Heat transfer equations.

Control volume	Heat transfer equations
Cathode interconnect	$\frac{1}{\alpha_{ci}} \cdot \frac{\partial T}{\partial t} = \frac{\partial^2 T}{\partial x^2} + \frac{\partial^2 T}{\partial y^2}$ $x = 0$ and $x = L \Rightarrow \frac{\partial T}{\partial x} = 0$, $y = 0 \Rightarrow \frac{\partial T}{\partial y} = 0$
	$y = t_{ci} \Rightarrow -k_{ci} \cdot \frac{\partial T}{\partial y} = \frac{w_{gas}}{w_{solid}} \cdot [h_{c,a} \cdot (T_{ci} - T_a) + h_{r,a} \cdot (T_{ci} - T_{PEN})] + \left(1 - \frac{w_{gas}}{w_{solid}}\right) \cdot k_{ci} \cdot \frac{(T_{ci} - T_{PEN})}{t_{ac}}$
	$t = 0 \Rightarrow T = T_o$
Air channel	$\rho_{ac} \cdot c_{p,ac} \cdot \frac{\partial T}{\partial t} + \sum_i \frac{\partial}{\partial x}(\dot{n}''_i \cdot \tilde{h}_i) = \frac{h_{c,a}(T_{PEN} - T_a) + h_{c,a}(T_{ci} - T_a) - (\dot{r}''_{el}/2) \cdot \tilde{h}_{O_2} \cdot (w_{solid}/w_{gas})}{t_{ac}}$
	$x = 0 \Rightarrow \begin{matrix} T = f(t)\,(\text{Heat-up}) \\ T = T_{w\_ac}\,(\text{Start-up}) \end{matrix}$ (co-flow), $x = L \Rightarrow \begin{matrix} T = f(t)\,(\text{Heat-up}) \\ T = T_{w\_ac}\,(\text{Start-up}) \end{matrix}$ (counter-flow)
	$t = 0 \Rightarrow T = T_o + 100\ ^\circ\text{C}$
PEN	$\frac{1}{\alpha_{PEN}} \cdot \frac{\partial T}{\partial t} = \frac{\partial^2 T}{\partial x^2} + \frac{\partial^2 T}{\partial y^2} + \frac{1}{k_{PEN}}\dot{q}'''_{PEN}$
	$x = 0$ and $x = L \Rightarrow \frac{\partial T}{\partial x} = 0$
	$y = t_{ci} + t_{ac} \Rightarrow k_{PEN} \cdot \frac{\partial T}{\partial y} = \frac{w_{gas}}{w_{solid}} \cdot [h_{c,a} \cdot (T_{PEN} - T_a) + h_{r,a} \cdot (T_{PEN} - T_{ci})] + \left(1 - \frac{w_{gas}}{w_{solid}}\right) \cdot k_{ci} \cdot \frac{(T_{PEN} - T_{ci})}{t_{ac}}$
	$y = t_{ci} + t_{ac} + t_{PEN} \Rightarrow -k_{PEN} \cdot \frac{\partial T}{\partial y} = \frac{w_{gas}}{w_{solid}} \cdot \left[h_{c,f} \cdot (T_{PEN} - T_f) + h_{r,f} \cdot (T_{PEN} - T_{ai})\right] + \left(1 - \frac{w_{gas}}{w_{solid}}\right) \cdot k_{ai} \cdot \frac{(T_{PEN} - T_{ai})}{t_{fc}}$
	$t = 0 \Rightarrow T = T_o$
Fuel channel	$\rho_{fc} \cdot c_{p,fc} \cdot \frac{\partial T}{\partial t} + \sum_i \frac{\partial}{\partial x}(\dot{n}''_i \cdot \tilde{h}_i) = \frac{h_{c,f}(T_{ai} - T_f) + h_{c,f}(T_{PEN} - T_f) + \left(\sum \dot{r}''_{prod} \cdot \tilde{h}_{prod} - \sum \dot{r}''_{react} \cdot \tilde{h}_{react}\right) \cdot w_{solid}/w_{gas}}{t_{fc}}$
	$x = 0 \Rightarrow T = Tw\_fc\,(\text{Start-up})\,(\text{co-flow})$, $x = L \Rightarrow T = Tw\_fc\,(\text{Start-up})\,(\text{counter-flow})$
	$t = 0 \Rightarrow T = T_o$
Anode interconnect	$\frac{1}{\alpha_{ai}} \cdot \frac{\partial T}{\partial t} = \frac{\partial^2 T}{\partial x^2} + \frac{\partial^2 T}{\partial y^2}$
	$x = 0$ and $x = L \Rightarrow \frac{\partial T}{\partial x} = 0$, $y = t_{ci} + t_{ac} + t_{PEN} + t_{fc} + t_{ai} \Rightarrow \frac{\partial T}{\partial y} = 0$
	$y = t_{ci} + t_{ac} + t_{PEN} + t_{fc} \Rightarrow -k_{ai} \cdot \frac{\partial T}{\partial y} = \frac{w_{gas}}{w_{solid}} \cdot \left[h_{c,f} \cdot (T_{ai} - T_f) + h_{r,f} \cdot (T_{ai} - T_{PEN})\right] + \left(1 - \frac{w_{gas}}{w_{solid}}\right) \cdot k_{ai} \cdot \frac{(T_{ai} - T_{PEN})}{t_{fc}}$
	$t = 0 \Rightarrow T = T_o$

Table 3
Auxiliary relations used in the modeling.

Name of the relation	Equation
Rate of electrochemical reaction	$\dot{r}''_{el} = \frac{i}{2F}$
Rate of steam reforming of methane [17]	$\dot{r}''_{str} = 4274 \cdot P_{CH_4} \cdot \exp\left(\frac{-8.2\times10^4}{R\times T}\right)$
Chemical equilibrium constant of water–gas shift reaction	$K_{wgs} = \exp\left[-\Delta\tilde{g}^{\circ}_{wgs}/RT\right] = \frac{x_{H_2}\cdot x_{CO_2}}{x_{CO}\cdot x_{H_2O}}$
Power density	$\dot{W}''_{el} = i \cdot V_{cell}$
Cell voltage	$V_{cell} = V_N - V_{ohm} - V_{act} - V_{con}$
Nernst voltage	$V_N = \frac{-\Delta\tilde{g}^{\circ}_r}{2F} - \frac{RT}{2F}\cdot\ln\left(\frac{P_{H_2O}}{P_{H_2}\cdot\sqrt{P_{O_2}/P^{\circ}}}\right)$
Ohmic polarization [18]	$V_{ohm} = \sum_k \rho_k \cdot L_k \cdot i$
Activation polarization [19]	$V_{act} = V_{act,a} + V_{act,c} = \frac{RT}{F}\cdot\sinh^{-1}\left(\frac{i}{2i_{o,a}}\right) + \frac{RT}{F}\cdot\sinh^{-1}\left(\frac{i}{2i_{o,c}}\right)$
Concentration polarization [20]	$V_{conc,a} = -\frac{RT}{2F}\ln\left(1-\frac{RT}{2F}\cdot\frac{\tau_a L_a}{D_a V_{v(a)} P^b_{H_2}} i\right) + \frac{RT}{2F}\ln\left(1+\frac{RT}{2F}\cdot\frac{\tau_a L_a}{D_a V_{v(a)} P^b_{H_2O}} i\right)$
	$V_{conc,c} = \frac{RT}{4F}\ln\left[\frac{P^b_{O_2}}{P-(P-P^b_{O_2})\exp\left[(RT/4F)\cdot(\tau_c l_c/D_c V_{v(c)} P)i\right]}\right]$
	$V_{conc} = V_{conc,a} + V_{conc,c}$
Volumetric heat generation in PEN	$\dot{q}'''_{PEN} = \frac{\sum \Delta\dot{H}''_k - \dot{W}''_{el}}{t_{PEN}}$
Reynolds number at the fuel channel inlet	$\mathrm{Re}_{D_h} = \frac{\dot{n}''_{k,fi}\cdot M_{mix}\cdot(2\cdot t_{fc}\cdot w_{gas})}{x_{k,fi}\cdot\mu_{mix}\cdot(t_{fc}+w_{gas})}$
Excess air coefficient	$\lambda_{air} = \frac{\dot{n}''_{O_2,ai}}{\left(2\cdot\dot{n}''_{CH_4,fi}+\dot{n}''_{CO,fi}/2+\dot{n}''_{H_2,fi}/2\right)}\cdot\frac{t_{ac}}{t_{fc}}$
Fuel utilization	$U_f = \frac{\sum_{i=2}^{m}\dot{r}''_{el}\cdot(\Delta x\cdot w_{solid})}{\left(4\cdot\dot{n}''_{CH_4,fi}+\dot{n}''_{H_2,fi}+\dot{n}''_{CO,fi}\right)\cdot(w_{gas}\cdot t_{fc})}$
Electrical efficiency	$\eta_{el} = \frac{\dot{W}_{SOFC}}{LHV\cdot\sum_{k=1}^{6}\dot{n}''_{k,fi}\cdot t_{fc}\cdot w_{gas}}$

Table 4
Material properties of the components of the PEN.

Component	Young's modulus/GPa	Poisson's coefficient	Coefficient of thermal expansion/K^{-1}	Characteristic strength/MPa	Weibull modulus	Reference volume/mm^3
Cathode (LSM)	35	0.360	11.7×10^{-6}	75	4	2.81
Electrolyte (YSZ)	190	0.308	10.8×10^{-6}	282	8	0.27
Anode (Ni–YSZ)	56.8	0.258	12.5×10^{-6}	187	11.8	0.578

Source: Laurencin et al. [14].

Table 5
Input data used in the benchmark test.

Cell geometry	
Active area/cm^2	10×10
Anode thickness/cm	0.005
Cathode thickness/cm	0.005
Electrolyte thickness/cm	0.015
Channel width/cm	0.3
Channel height/cm	0.1
Rib width/cm	0.242
Total thickness (with ribs)/cm	0.25
Operating parameters	
Temperature at the fuel channel inlet/°C	900
Temperature at the air channel inlet/°C	900
Pressure of the cell/kPa	100
Excess air coefficient	7
Fuel utilization	0.85
Mean current density/A cm^{-2}	0.3
Gas composition at the air channel inlet	21% O_2, 79% N_2
Gas composition at the fuel channel inlet	17.1% CH_4, 26.26% H_2, 2.94% CO, 4.36% CO_2, and 49.34% H_2O

Source: Achenbach [22].

Table 6
Validation of the Model-V1 and Model-V2 of the co-flow configuration with the benchmark test and Braun's model.

Parameter	Co-flow			
	Benchmark[a]	Braun's model[b]	Model-V1[c]	Model-V2[d]
	Max/Min			
Voltage/V	0.65/0.63	0.65	0.65	0.65
Power/W	19.47/18.99	19.49	20.15	21.92
Efficiency/%	N/A	49.8	49.5	49.8
Current density/A cm^{-2}				
Max	0.367/0.304	0.346	0.360	0.448
Min	0.251/0.175	0.215	0.216	0.174
Solid temperature/°C				
Max	1034/1021	1020	1025	1023
Min	862/847	845	853	858
Outlet gas temperature/°C	Max/Min			
Air	1026/1016	1014	1022	1022
Fuel	1026/1021	1019	1024	1023

[a] Data show the results from the benchmark test. Data are taken from Braun's thesis [23].
[b] Data show the results from the Braun's model. Data are taken from Braun's thesis [23].
[c] Data show the results from the present model that uses the same assumption with the benchmark test.
[d] Data show the results from the present model that uses the different assumption for polarizations.

by International Energy Agency [22], and two numerical studies using the same input data and assumptions with the benchmark test (Braun [23] and Selimovic et al. [1]). In the benchmark test, several companies and institutions modeled planar DIR-SOFC using the same operating data, which are shown in Table 5.

The main assumption used in the benchmark test was to accept each of the polarizations in the anode and cathode as equal to the ohmic loss of the electrolyte. In this study, a heat transfer model has been first developed using the same assumption for polarizations as the benchmark tests. This model is called Model-V1. This assumption is then altered in that different analytical equations are considered for ohmic, activation and concentration polarizations, which are shown in Table 3. This model is called Model-V2. In addition, some input and output parameters of this model are considered different than the models developed in the benchmark test. As opposed to the benchmark test, fuel utilization and average current density are taken as output parameters; whereas the cell voltage and Reynolds number are taken as input parameters in this model. The model is validated for the steady-state condition using the results of the benchmark test [22] and Braun's model [23], and for the transient condition using the results of the study by Selimovic et al. [1].

The results of the benchmark test were given for fuel utilization of 0.85 and an average current density of 0.3 A cm^{-2}. Since these two parameters are output parameters in the model developed by the authors, Reynolds number is altered until we get results that are close enough to these two parameters. For the co-flow configuration, Reynolds number is found to be 1.85 in the Model-V1, which gives fuel utilization of 0.85 and average current density of 0.318 A cm^{-2}. For the same configuration in Model-V2, Reynolds number is found to be 2, which gives fuel utilization of 0.85 and average current density of 0.346 A cm^{-2}. For the counter-flow configuration, in the Model-V1 and Model-V2, Reynolds number is found to be 1.7, which gives fuel utilization of 0.85 and average current density of 0.3 A cm^{-2}.

The validation of the co-flow configuration for the Model-V1 and Model-V2 is given in Table 6. As the cell voltage is an input parameter in the model developed by the authors, a value between the maximum and minimum values of the cell voltage from the models conducted in the benchmark test is taken, as shown in this table. From this table, it can be seen that the results for the Model-V1 is between the maximum and minimum values found by the companies and institutions participated in the benchmark test except the power. The result for the power has a relative error of 3.37% and 5.76% with the maximum and minimum value of the power found by the participants of the benchmark test, respectively. For Model-V2 of the co-flow case, the maximum current density is slightly higher than the maximum value of the benchmark test, as shown in this table, because of the assumption on the polarizations done in this model.

The validation of the counter-flow configuration for the Model-V1 and Model-V2 is given in Table 7. When we check the results from this table, we see that the results for Model-V1 are slightly lower than the values given for the benchmark test. This difference is mainly due to the methodology applied in the modeling. In the model developed by the authors, outlet of fuel channel and inlet of air channel temperatures are considered fixed; whereas it is not clear what kind of an assumption is done in the models developed in the benchmark test. In spite of this assumption, the relative errors for Model-V1 for power, maximum current density, minimum current density, maximum solid temperature, minimum solid temperature, exit temperature of air channel and exit temperature of fuel channel are 0.99%, 2.30%, 4.72%, 2.91%, 0.11%, 3.67% and 0.67%, respectively. The results for Model-V2 are almost same with the Model-V1 except the maximum and minimum values of current density. This difference is due to the difference on the assumption on polarizations between these two models. However, the average current densities for these two models are found as same, which are equal to 0.3 A cm^{-2}.

The results for the distribution of the output parameters could not be accessed for the benchmark test. However, those results for the co-flow configuration from Braun's study are used for valida-

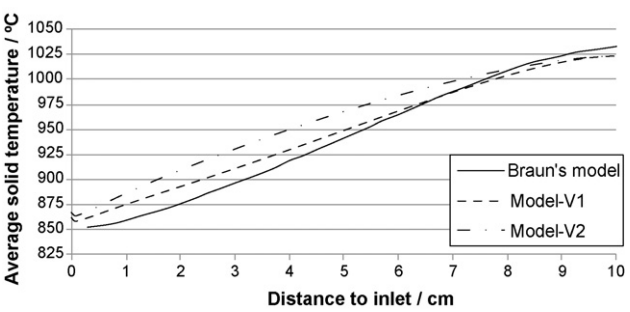

Fig. 2. Validation for the distribution of the average solid temperature.

Table 7
Validation of the Model-V1 and Model-V2 of the counter-flow configuration with the benchmark test and Braun's model.

Parameter	Counter-flow			
	Benchmark[a]	Braun's model[b]	Model-V1[c]	Model-V2[d]
	Max/Min			
Voltage/V	0.692/0.680	0.693	0.69	0.69
Power/W	20.76/20.40	20.78	20.2	20.2
Efficiency/%	N/A	53.1	52.7	52.6
Current density/A cm^{-2}				
Max	0.655/0.533	0.540	0.521	0.444
Min	0.133/0.099	0.126	0.127	0.169
Solid temperature/°C				
Max	1089/1062	1058	1032	1033
Min	915/906	912	907	909
Outlet gas temperature/°C	Max/Min			
Air	1028/1018	1014	982	981
Fuel	915/906	914	900	900

[a] Data show the results from the benchmark test. Data are taken from Braun's thesis [23].
[b] Data show the results from the Braun's model. Data are taken from Braun's thesis [23].
[c] Data show the results from the present model that uses the same assumption with the benchmark test.
[d] Data show the results from the present model that uses the different assumption for polarizations.

tion of the distribution of average solid temperature and current density. It can be seen from Figs. 2 and 3 that these distributions for Model-V1 and Braun's study have similar trends. The current density distribution for Model-V2 is different, which is due to the nature of equations used for calculating the polarizations.

The validation of the transient behavior of the cell is done using the results of the study by Selimovic et al. [1]. In their study, they used the assumptions and input data taken from the benchmark test. They showed the change of average solid temperature with time during the start-up period. They considered the value of the average solid temperature at the beginning of the start-up period as 700 °C. Considering this value, Model-V1 and Model-V2 are simulated to validate the transient behavior of the cell. As shown in Fig. 4, the time that the cell starts to operate at steady state, and the trend of the change of temperature are very similar between the models developed by the authors and Selimovic et al.'s model. The difference between these models could arise from the fact that Selimovic et al. used a simpler thermal model assuming the solid temperature as homogeneous in each volume element.

4.2. Heat-up, start-up, and steady-state behaviors of the cell

After validating the model, the co- and counter-flow simulations are carried out for the same cell voltage and fuel utilization, which are chosen as 0.69 V and 0.85, respectively. For obtaining this fuel utilization, Reynolds number at the fuel channel inlet is found as 1.55 for co-flow and 1.7 for counter-flow configuration. Heat-up time for both of these configurations is found as 794 s. The steady-state condition is satisfied at 4433 s for co-flow, and 4493 s for counter-flow configuration, respectively.

The heat-up period continues until the minimum solid temperature becomes 700 °C. At this value, the ohmic polarization of the electrolyte becomes low enough; hence a meaningful amount of power can be produced from the cell. A step change of the temperature of the air channel inlet is considered at this period since the difference between the air channel inlet temperature and minimum solid temperature should not exceed 100 °C. The mass flow rate per cross-section of the air channel, which is taken as 2.373 g s^{-1} cm^{-2} in this study, is the main parameter affecting the duration of this period. The value of this parameter should be taken high enough to reduce the heat-up time. However, an increase in its value causes an increase in the power demand of the blower; which in turn decreases the electrical efficiency of the fuel cell system. In modeling the start-up period, this parameter is non-dimensionalized using excess air coefficient, which is taken as 7 in the calculations. In general, this coefficient should be taken high enough not to cause excessive thermal stresses within the cell, and low enough to have a high exit temperature which is especially important if the SOFC is integrated with bottoming cycles. Considering these facts, changes of temperature in the heat-up and start-up periods with time are calculated. Figs. 5–7 show the change of average solid temperature, air channel outlet, and fuel channel inlet/outlet temperatures with time, respectively. As it can be seen from these figures, there is not a significant difference between co- and counter-flow configurations.

Figs. 8 and 9 show how the fuel utilization, average current density, electrical efficiency and power density change with time for the co-flow and counter-flow configurations. As it can be seen from

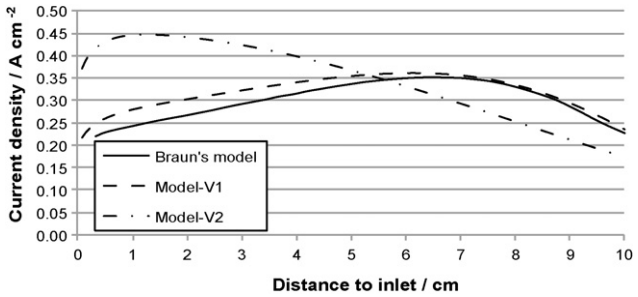

Fig. 3. Validation for the distribution of the current density.

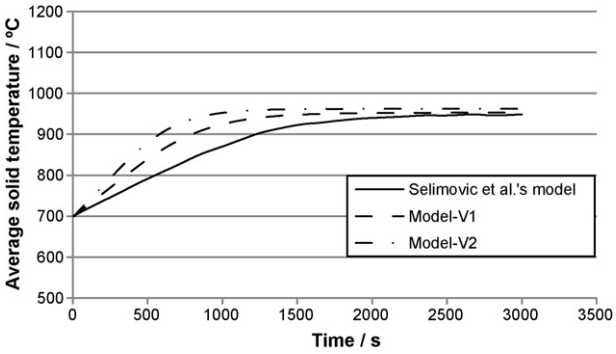

Fig. 4. Validation of the transient behavior of the cell.

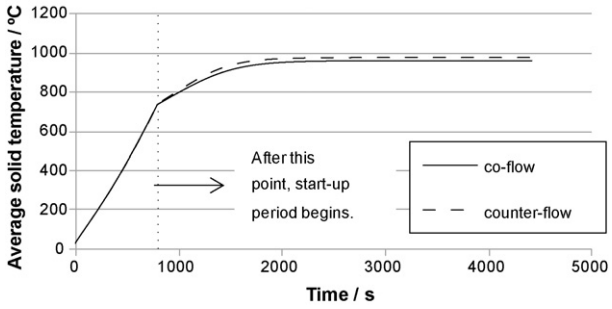

Fig. 5. Change of average solid temperature with time for the DIR-SOFC (for the cell voltage of 0.69 V and the fuel utilization of 0.85).

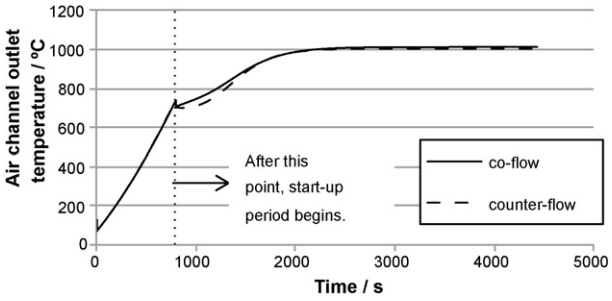

Fig. 6. Change of air channel outlet temperature with time for the DIR-SOFC (for the cell voltage of 0.69 V and the fuel utilization of 0.85).

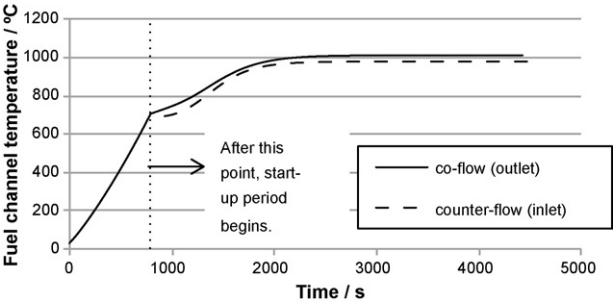

Fig. 7. Change of fuel channel temperature with time for the DIR-SOFC (for the cell voltage of 0.69 V and the fuel utilization of 0.85).

these figures, the values of these parameters are zero during the heat-up period because electrochemical reactions do not occur in this period since there is no flow in the fuel channel. As the start-up period begins, their values increase gradually because of the increase in the temperature, which enhances the performance of the cell; and then they become constant when the system reaches steady state. For example, as can be followed from these figures,

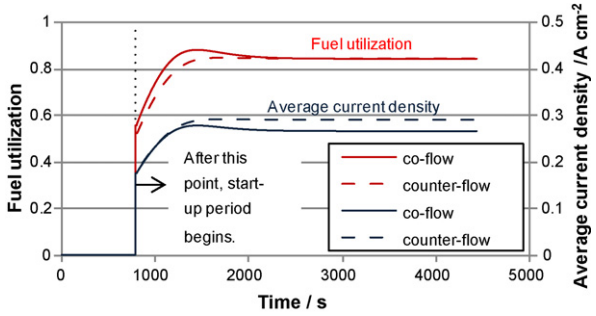

Fig. 8. Change of fuel utilization and average current density with time for the DIR-SOFC (for the cell voltage of 0.69 V and the fuel utilization of 0.85).

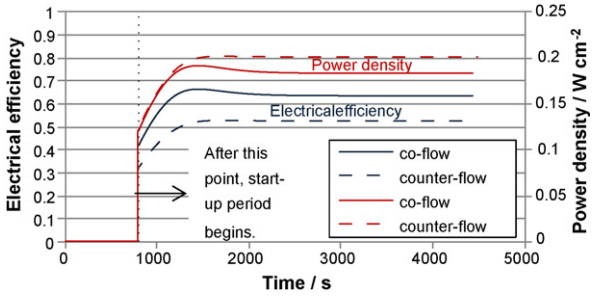

Fig. 9. Change of electrical efficiency and power density with time for the DIR-SOFC (for the cell voltage of 0.69 V and the fuel utilization of 0.85).

during the start-up period of the co-flow case, average current density, fuel utilization, power density, and electrical efficiency increase from 0.18 to 0.27 A cm^{-2}, 0.56 to 0.85, 0.12 to 0.18 W cm^{-2}, and 0.42 to 0.63, respectively. When the co- and counter-flow cases are compared for the same cell voltage and fuel utilization, it can be seen that counter-flow case has a higher average current density, mainly because of the higher Reynolds number (or higher mass flow rate of fuel) at the fuel channel inlet for this case. Since we fix the cell voltage for comparison, power density is directly proportional to the average current density. Due to that reason, counter-flow case has also a higher power density. Electrical efficiency of the cell mainly depends on the power density and the total molar flow rate at the fuel channel inlet. As we need to send more fuel for the counter-flow case to get the same fuel utilization, the electrical efficiency for the co-flow case becomes higher although the power density is lower for this case.

Figs. 10 and 11 show the distribution of molar gas composition of gas species in the fuel channel at the steady-state condition for the co- and counter-flow configurations, respectively. As can be from these figures, up to a point close to the inlet, the trend of the

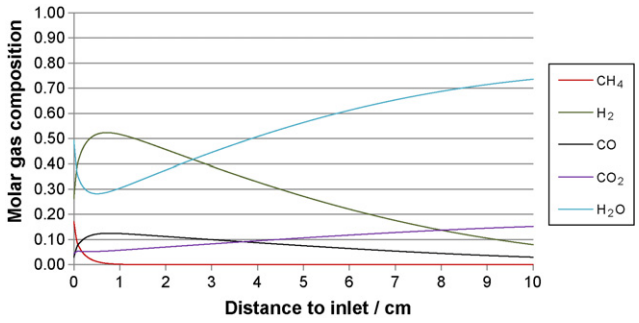

Fig. 10. Distribution of molar composition of gas species in the fuel channel of the co-flow DIR-SOFC at the steady-state condition (for cell voltage of 0.69 V and fuel utilization of 0.85).

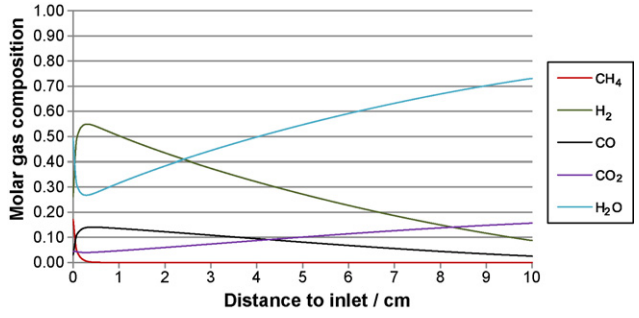

Fig. 11. Distribution of molar composition of gas species in the fuel channel of the counter-flow DIR-SOFC at the steady-state condition (for cell voltage of 0.69 V and fuel utilization of 0.85).

composition of the gas species is different from the remaining part of the gas channel. This trend is due to the fact that methane is fully consumed at this point, hence steam reforming of methane reaction do not occur anymore after this point. The only reactions affecting the molar compositions in the remaining part of the cell are the electrochemical reaction and the water–gas shift reaction. As the rate of steam reforming of methane is proportional to temperature and the temperature at the inlet of the counter-flow case is higher, the point at which methane is fully consumed is closer to the inlet for the counter-flow case, as shown in these figures.

Figs. 12 and 13 show the temperature distribution within the cell at the steady-state condition for co- and counter-flow configurations, respectively. As can be followed from Fig. 12, the temperature at the flow direction drops suddenly due to the endothermic steam reforming reaction and then increases through the channel due to exothermic electrochemical and water–gas shift reactions. In the counter-flow case, as the temperatures of the exit of the fuel channel and the inlet of the air channel are fixed, the temperature rise occurs in the opposite direction compared to the co-flow case. The effect of steam reforming reaction can also be seen for this case since there is a sudden temperature drop close to the inlet of the cell.

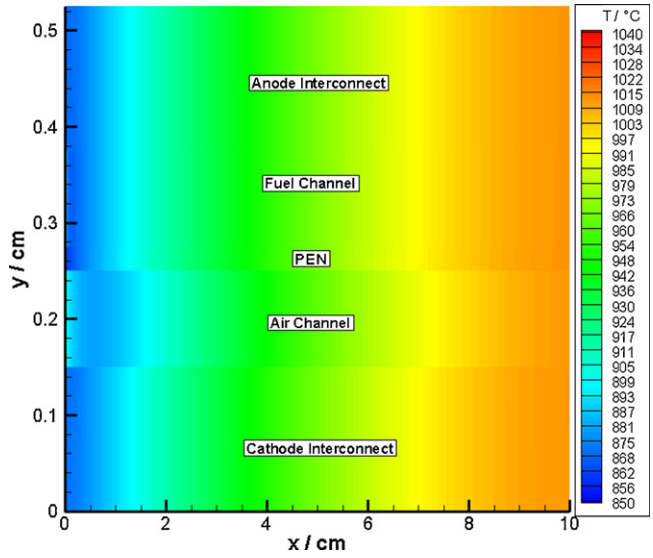

Fig. 12. Temperature distribution in the co-flow DIR-SOFC at the steady-state condition (for cell voltage of 0.69 V and fuel utilization of 0.85).

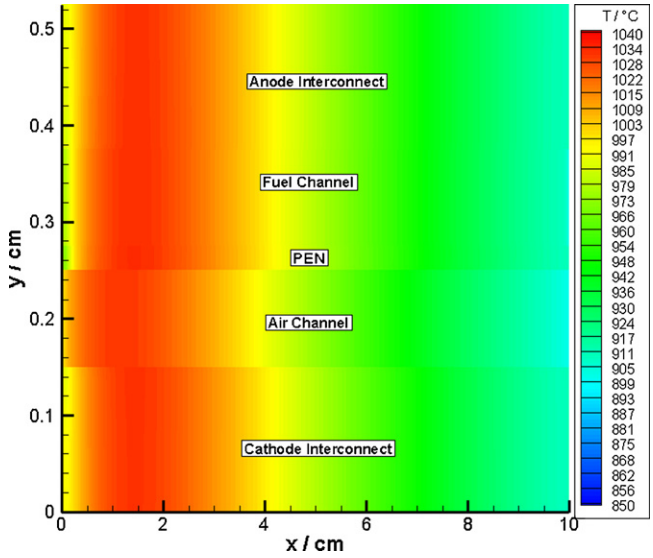

Fig. 13. Temperature distribution in the counter-flow DIR-SOFC at the steady-state condition (for cell voltage of 0.69 V and fuel utilization of 0.85).

4.3. Probability of failure of the cell during its operation

The first principal thermal stresses formed within the cell are found; and these stresses are used to calculate the probability of failure of PEN during the heat-up and start-up periods of the cell. As can be seen from Fig. 14, the probability of failure is lower than 0.01% at the heat-up period mainly because of using a controlled air inlet temperature at this period. The trend of this probability for the heat-up period may be seen controversial when it is compared to the findings of some of the papers found in the literature, e.g. Ref. [24]. It was shown that the failure probability becomes maximum at the beginning of the heat-up period. The reason of their finding is that they studied the operation of SOFC right after its assembly. They considered that the cell is stress-free at the assembly temperature, e.g. 800 °C because of the uniform temperature distribution of the cell. The thermal stresses formed due to cooling the cell from the assembly temperature to room temperature, which can also be named as shut-down period, were first calculated. Then, these stresses were considered as the initial stresses in the heat-up simulation. However, in the present study, it is assumed that the cell has already been assembled and cooled to room temperature a sufficiently long time ago to consider the cell as thermal stress-free at this temperature.

At the start-up period, the chemical and electrochemical reactions cause higher temperature gradients; which in turn increases the value of the probability of failure. It is found that this value increases up to 0.068% and 0.078% during the start-up period for co- and counter-flow configurations, respectively. It should be noted that the probability of failure for electrolyte is always found to be greater than that for anode and cathode. For example, this probability changes in the order of 10^{-15} to 10^{-12}, 10^{-11} to 10^{-7}, and 10^{-12} to 10^{-4} for anode, cathode, and electrolyte, respectively, during the operation of the cell.

Figs. 15 and 16 show the first principal thermal stress distributions in the PEN structure for co- and counter-flow configurations, respectively, when the system reaches the steady-state condition. As can be seen from these figures, the maximum stress occurs at a point close to the inlet of the fuel channel and the interface of the anode and electrolyte for both configurations. The main reasons of this finding are that the endothermic steam reforming reaction of methane causes a high temperature gradient at this point and the thermal expansion coefficient difference between the anode and electrolyte is higher compared to that of cathode and electrolyte. The value of the maximum stress is found as 102.763 MPa and 99.833 MPa for the co- and counter-flow configurations, respectively.

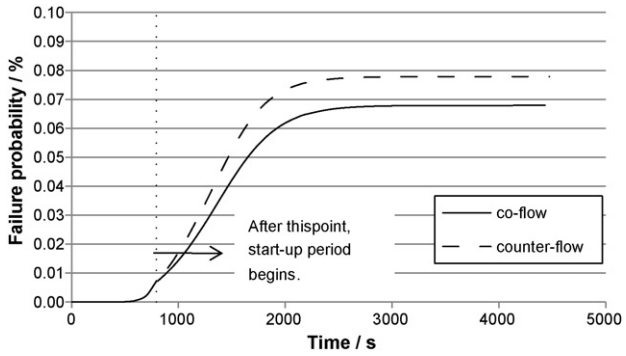

Fig. 14. Failure probability of PEN during the cell operation.

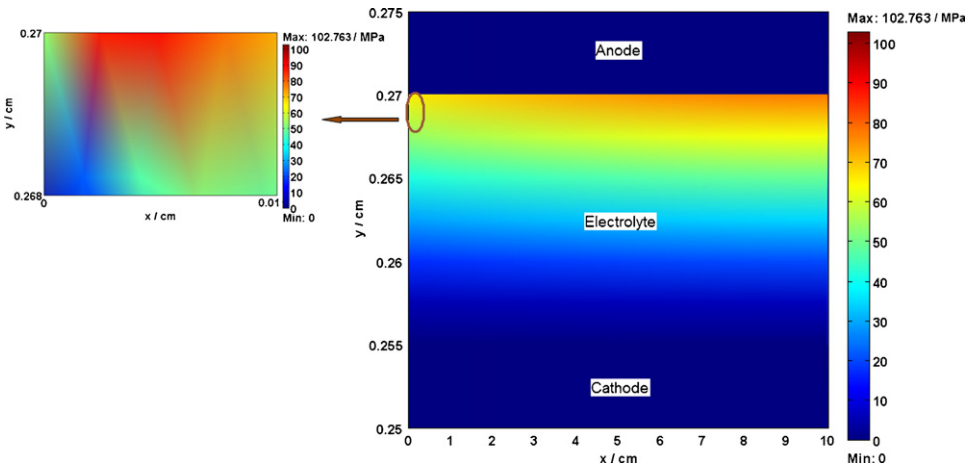

Fig. 15. The first principal stress distribution in the co-flow DIR-SOFC at the steady-state condition (for cell voltage of 0.69 V and fuel utilization of 0.85).

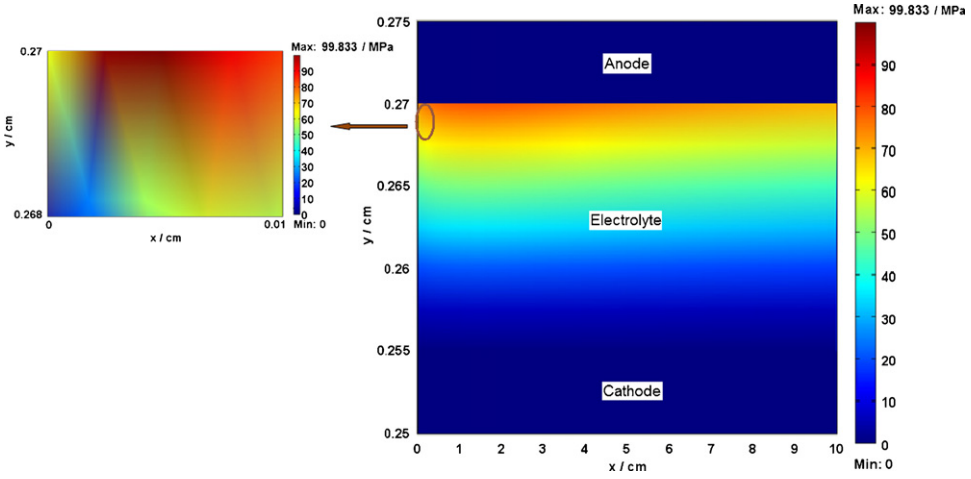

Fig. 16. The first principal stress distribution in the counter-flow DIR-SOFC at the steady-state condition (for cell voltage of 0.69 V and fuel utilization of 0.85).

5. Conclusions

A comprehensive model has been developed to study the heat-up and start-up periods of the co- and counter-flow DIR-SOFCs. This model includes all the heat transfer mechanisms (e.g. conduction, convection and radiation) and all the polarizations nodes (e.g. ohmic, activation and concentration). The results of a benchmark test and two numerical models found in the literature are used for validation purposes. It is found that the results are in good agreement. After validating the model, the transient (heat-up and start-up) and steady-state behavior of the cell are investigated; and a comparison between co- and counter-flow configurations are done for the same cell voltage and fuel utilization. For the given data, the results show that counter-flow case yields a higher average current density and power density, but a lower electrical efficiency of the cell. The temperature distribution obtained using the transient heat transfer model is used to calculate the first principal thermal stresses and the probability of failure of the PEN during the operation of the cell. It is found that the maximum stress occurs at a point close to the fuel channel inlet and the interface of anode and electrolyte; and the probability of failure is higher for counter-flow configuration for the input data considered in this study.

In the future, a parametric study will be undertaken to investigate the effect of design and operation parameters of the cell on the transient behavior and the probability of failure of the PEN. Further improvements are expected in the current modeling including the interactions between the adjacent repeat elements, and other failure modes, e.g. anode/electrolyte interfacial delamination.

Acknowledgements

The financial and technical support of an Ontario Premier's Research Excellence Award, the Natural Sciences and Engineering Research Council of Canada, Carleton University and University of Ontario and Institute of Technology is gratefully acknowledged.

References

[1] A. Selimovic, M. Kemm, T. Torisson, M. Assadi, Journal of Power Sources 145 (2005) 463–469.
[2] L. Petruzzi, S. Cocchi, F. Fineschi, Journal of Power Sources 118 (2003) 96–107.
[3] Y. Choux, J. Chen, T. Chung, Journal of The Electrochemical Society 155 (7) (2008) B650–B659.
[4] C.O. Colpan, I. Dincer, F. Hamdullahpur, International Journal of Hydrogen Energy 32 (2007) 787–795.
[5] J. Li, G. Cao, X. Zhu, H. Tu, Journal of Power Sources 171 (2007) 585–600.
[6] H. Yakabe, T. Ogiwara, M. Hishinuma, I. Yasuda, Journal of Power Sources 102 (2001) 144–154.
[7] S. Farhad, F. Hamdullahpur, Journal of Power Sources 191 (2009) 407–416.
[8] C.O. Colpan, Y. Yoo, I. Dincer, F. Hamdullahpur, Environmental Progress & Sustainable Energy 28 (3) (2009) 380–385.
[9] C.O. Colpan, F. Hamdullahpur, I. Dincer, Y. Yoo, International Journal of Hydrogen Energy, in press.

[10] C.O. Colpan, I. Dincer, F. Hamdullahpur, International Journal of Energy Research 32 (2008) 336–355.
[11] D.L. Damm, A.G. Fedorov, Journal of Power Sources 159 (2006) 956–967.
[12] P. Aguiar, C.S. Adjiman, N.P. Brandon, Journal of Power Sources 147 (2005) 136–147.
[13] T. Zhang, Q. Zhu, W.L. Huang, Z. Xie, X. Xin, Journal of Power Sources 182 (2008) 540–545.
[14] J. Laurencin, G. Delette, F. Lefebvre-Joud, M. Dupeux, Journal of the European Ceramic Society 28 (2008) 1857–1869.
[15] D. Cui, M. Cheng, Journal of Power Sources 192 (2009) 400–407.
[16] A. Nakajo, Z. Wuillemin, J. Van herle, D. Favrat, Journal of Power Sources 193 (2009) 203–215.
[17] E. Achenbach, Journal of Power Sources 49 (1994) 333–348.
[18] U.G. Bossel, Final Report on SOFC Data Facts and Figures, Swiss Federal Office of Energy, Berne, CH, 1992.
[19] S.H. Chan, Z.T. Xia, Journal of Applied Electrochemistry 32 (2002) 339–347.
[20] J. Kim, A.V. Virkar, K. Fung, K. Mehta, S.C. Singhal, Journal of the Electrochemical Society 146 (1) (1999) 69–78.
[21] W. Weibull, Journal of Applied Mechanics 18 (3) (1951) 293–297.
[22] E. Achenbach, SOFC Stack Modelling, Final Report of Activity A2, Annex II: Modelling and Evaluation of Advanced Solid Oxide Fuel Cells, International Energy Agency Programme on R, D&D on Advanced Fuel Cells, Juelich, Germany, 1996.
[23] R.J. Braun, Optimal Design and Operation of Solid Oxide Fuel Cell Systems for Small-Scale Stationary Applications, Ph.D. Thesis, University of Wisconsin-Madison, 2002.
[24] C. Lin, T. Chen, Y. Choux, L. Chiang, Journal of Power Sources 164 (2007) 238–251.